RSC Advances

PAPER

View Article Online
View Journal | View Issue

Cite this: *RSC Adv.*, 2019, **9**, 31867

Synthesis and application of amine-containing conjugated small molecules for the automatic formation of an electron transporting layer *via* spontaneous phase separation from the bulk-heterojunction layer†

Juae Kim,‡[a] Yong Ryun Kim,‡[b] Minji Kim,[a] Jong Sung Jin,[c] Ji Yeong Sung,[c] Hyungcheol Back,[b] Heejoo Kim,*[d] Kwanghee Lee *[e] and Hongsuk Suh *[a]

Carbazole-based conjugated small molecule electrolytes (CSEs) containing different numbers of amine groups were synthesized and applied to bulk-heterojunction (BHJ) organic solar cells for the formation of a spontaneous self-assembled electron transporting layer (ETL). The active layer was spin-coated with a mixture solution containing the BHJ materials and a small amount of CSE, and a thin layer of CSE was formed underneath the active layer (CSE/BHJ bi-layer) *via* spontaneous phase separation, which is confirmed by the depth profile of the time of flight secondary ion mass spectroscopy (ToF-SIMS) spectrum. The amino groups in the CSEs form hydrogen-bonds with the surface of indium tin oxide (ITO), which acts as an ETL in BHJ solar cells. Moreover, the formed CSE layer is capable of changing the effective work function (WF) of ITO. An increasing number of amino groups in the CSEs (from **Cz1N** to **Cz3N**) provides more reduction of the effective WF of ITO, which results in a lower internal resistance and a higher power conversion efficiency (PCE). Furthermore, the enhanced hydrogen bonding between the amines and ITO with an increased number of amine groups has been studied by XPS. This result suggests that one-step processing provides a reduction of the manufacturing cost, which can provide an attractive design concept for ETL fabrication.

Received 13th August 2019
Accepted 27th September 2019

DOI: 10.1039/c9ra06293a

rsc.li/rsc-advances

Introduction

Over the past decade, bulk-heterojunction (BHJ) solar cells comprising conjugated polymer donors and fullerene acceptors have attained significant attention due to their advantages, such as solution processability, large area fabrication, and applicability for roll-to-roll processes.[1–4] The improvement of the power conversion efficiency (PCE) of BHJ solar cells has been achieved through several strategies, such as control of BHJ morphology, new molecular design of the semiconducting materials, and modification of the interfaces.[5–12] Among them, introduction of interlayer materials between the indium tin oxide (ITO) bottom electrode and the photoactive layer in an inverted BHJ solar cell is regarded as one of the facile and efficient methods of improving the PCE of BHJ solar cells.[13–16] The introduced layer can generate an interfacial dipole at the interface to change the WF of the electrode, leading to ohmic contact between the BHJ layer and ITO. As a result, the electron transfer from the photoactive layer to the ITO electrode is facilitated, increasing the PCE.[13,15,17]

Solution processable metal oxides such as ZnO[18] and TiO_2 ref. 19 and [20] are the most popular electron transport layer (ETL) materials. However, their complicated fabrication method, with the application of a high annealing temperature (>200 °C) for the crystallization of the metal oxides, is not compatible with roll-to-roll manufacturing processes for high throughput.[18,21] To solve this problem, there is an alternative route without thermal annealing that is afforded by a ZnO nanoparticle (ZnO NP) emulsion, which allows applications in roll-to-roll deposition.[22,23] However, this sequential process for fabricating the ETL/BHJ bi-layered structure increases the number of fabrication steps for multi-layered devices, and thus is also unfavorable for the mass production of BHJ solar cells. As a low temperature processable ETL, polyelectrolytes such as

[a]*Department of Chemistry, Chemistry Institute for Functional Materials, Pusan National University, Busan 609-735, Republic of Korea. E-mail: hssuh@pusan.ac.kr*
[b]*Research Institute for Solar and Sustainable Energies, Gwangju Institute of Science and Technology, Gwangju 61005, Republic of Korea*
[c]*Busan Center, Korea Basic Science Institute (KBSI), Busan 46742, Republic of Korea*
[d]*Institute of Integrated Technology, Gwangju Institute of Science and Technology, Gwangju 61005, Republic of Korea. E-mail: heejook@gist.ac.kr*
[e]*School of Materials Science and Engineering, Gwangju Institute of Science and Technology, Gwangju 61005, Republic of Korea. E-mail: klee@gist.ac.kr*

† Electronic supplementary information (ESI) available: DSC and TGA curves, electrochemical characteristics, XRD powder patterns, device performance, solubility studies, and ^{1}H and ^{13}C NMR spectra. See DOI: 10.1039/c9ra06293a

‡ Contributed equally to this work.

poly[(9,9-bis(3′-(*N*,*N*-dimethylamino)propyl)-2,7-fluorene)-*alt*-2,7-(9,9-dioctylfluorene)] (PFN)[24] and polyethyleneimine ethoxylated (PEIE)[25] have been shown to be alternative candidates. Furthermore, their electronic structure can be easily tailored for ohmic contact at the interface by changing the polymer backbone or side chains.[26–35] However, polyelectrolytes/BHJ bi-layer structures are also fabricated with a sequential process.

Recently, Lee *et al.* reported a one-step process for fabricating an ETL/BHJ bi-layered structure, which is enabled by using a mixed BHJ solution including a small amount of non-conjugated polyethyleneimine (PEI). The amines in the PEI could induce spontaneous phase migration to ITO during the spin-casting due to the hydrogen bonding between PEI and ITO, thereby forming an ETL/BHJ bi-layered structure simply by using one spin-casting process.[36–38] Subsequently, a dipole layer is formed between the migrated PEI molecules and the surface of ITO, resulting in similar device performance to that of sequentially processed devices. However, as observed in the sequentially processed bi-layered devices, the optimized thickness of the PEI layer for the one-step processed BHJ solar cells was less than 5 nm.[39] Because the backbone of PEI is an insulating material causing thickness sensitivity, a thicker PEI layer (>5 nm) causes poor charge transport, decreasing both FF and JSC significantly. This result can be ascribed to a lack of conjugation portion in the polymer backbone of PEI.[40–43] Recently, Kim *et al.* reported self-organization of polymer additive poly(2-vinylpyridine) (P2VP) *via* one-step solution processing to increase the device performance. But P2VP was used in addition to a metal oxide (ZnO) layer, and could not reduce the processing steps of the device.[44] In contrast to the aforementioned works, Cao *et al.* reported a good device performance with a thicker ETL (thickness $\sim$ 40 nm)/BHJ bi-layered structure when they used a conjugated polyelectrolyte (CPE) as the ETL.[45] Although this bi-layered structure was fabricated by a sequential process, this result implies that CPEs comprising a conjugated portion and hydrophilic amine groups made it possible to keep the charge transport property.

Here, we report the design, syntheses and properties of novel conjugated small molecule electrolytes (CSEs), which have not only a conjugated portion for efficient electron transport but also amine groups, essential functional group of PEI for spontaneous phase separation. These CSEs with a carbazole moiety and amine groups have a simple synthetic method, batch-to-batch reproducibility, a well-defined molecule structure and absolutely fixed molecular weight. Carbazole was used as the conjugated moiety because it has been widely utilized as an ETL material. The hydrophobic carbazole portion will provide reasonable solubility of the CSEs in the solvent that is being used for the spin-coating of one solution of electron donor/electron acceptor/CSE. The amine groups provide the driving force for spontaneous phase separation to form a CSE layer on top of ITO.

Furthermore, we systemically studied the spontaneous phase separation of **CzxN** as an ETL in inverted organic solar cells by using one spin-coating method using one solution of PTB7-Th/$PC_{71}BM$/**CzxN**. With the aim of achieving better device performance, we chose to vary the number of amines to provide **Cz1N**, **Cz2N**, and **Cz3N**, since the variation of the number of amine groups can improve the hydrophilicity of the CSE. Furthermore, Kelvin probe (KP) measurement was used to check how the number of amines varies the WF of ITO cathodes. In addition to this, the hydrogen bonding between the amine and ITO after spontaneous phase separation has been confirmed by XPS.

The KP measurements on **CzxN**/ITO showed that the WF of ITO decreased on increasing the number of amine groups. The water contact angle measurements on **CzxN** and BHJ : **CzxN** films showed that the hydrophilic properties of CSEs were improved on increasing the number of amine groups in the CSEs. A higher performance was obtained with the device with an increased number of amine groups (**Cz3N**), which provided a lower WF of ITO, lower water contact angle and more efficient hydrogen bonding with ITO as confirmed by XPS. Therefore, our results will provide a way of developing effective ETL materials inducing spontaneous phase separation to realize a printing process of large area BHJ solar cells with reduced steps.

Results and discussion

Material characterization

The general synthetic routes toward the intermediates and small molecules are outlined in Scheme 1. The detail synthetic routes are described in the experimental section and the ESI.† 9-(6-Bromo-hexyl)-9*H*-carbazole (**2**) was synthesized by alkylation of 9*H*-carbazole (**1**). **Cz1N** was prepared by amination of compound **2**. After the Kornblum oxidation of compound **2**, 6-carbazol-9-yl-hexanal (**3**) was obtained. **Cz2N** and **Cz3N** were synthesized by reductive amination of the aldehyde with a carbazole moiety using the corresponding amine-containing reagents. All of the final compounds, which have simple synthetic routes and can be easily purified, dissolve in polar solvents such as MeOH. The clear identifications of the synthesized molecules were performed by using ^{1}H NMR, ^{13}C NMR and mass spectrometry as shown in the ESI, Fig. S1–S3.†

The UV-vis absorption spectra of the solutions (in MeOH) and solid films of **CzxN**s are presented in Fig. S4† and the λ_{max} values both for solutions and solid films are summarized in Table S1.† As shown in Fig. S4(a),† the solutions of **CzxN**s in MeOH exhibited almost identical absorption spectra with peaks at 330 nm and 345 nm. In solid films, the wavelength of the optical absorption onset was slightly red-shifted from 356 nm to 358 nm on increasing the number of amine groups. Therefore, the optical band gaps for **Cz1N**, **Cz2N**, and **Cz3N** were estimated to be 3.48, 3.47 and 3.46 eV, respectively. Nevertheless, the shapes of the absorption spectra for all solid films were almost identical, indicating that the change of the side chains does not disturb the electronic structure of the carbazole moiety. The electrochemical properties of the **CzxN** molecules, such as the highest occupied molecular orbital (HOMO) and lowest unoccupied molecular orbital (LUMO) energy levels, were characterized by using cyclic voltammetry (CV) (see Fig. S5† and Table S2†). The HOMO and LUMO energy levels of **Cz1N**, **Cz2N** and **Cz3N** were estimated to be −6.99, −7.03, −7.04 eV and −3.19,

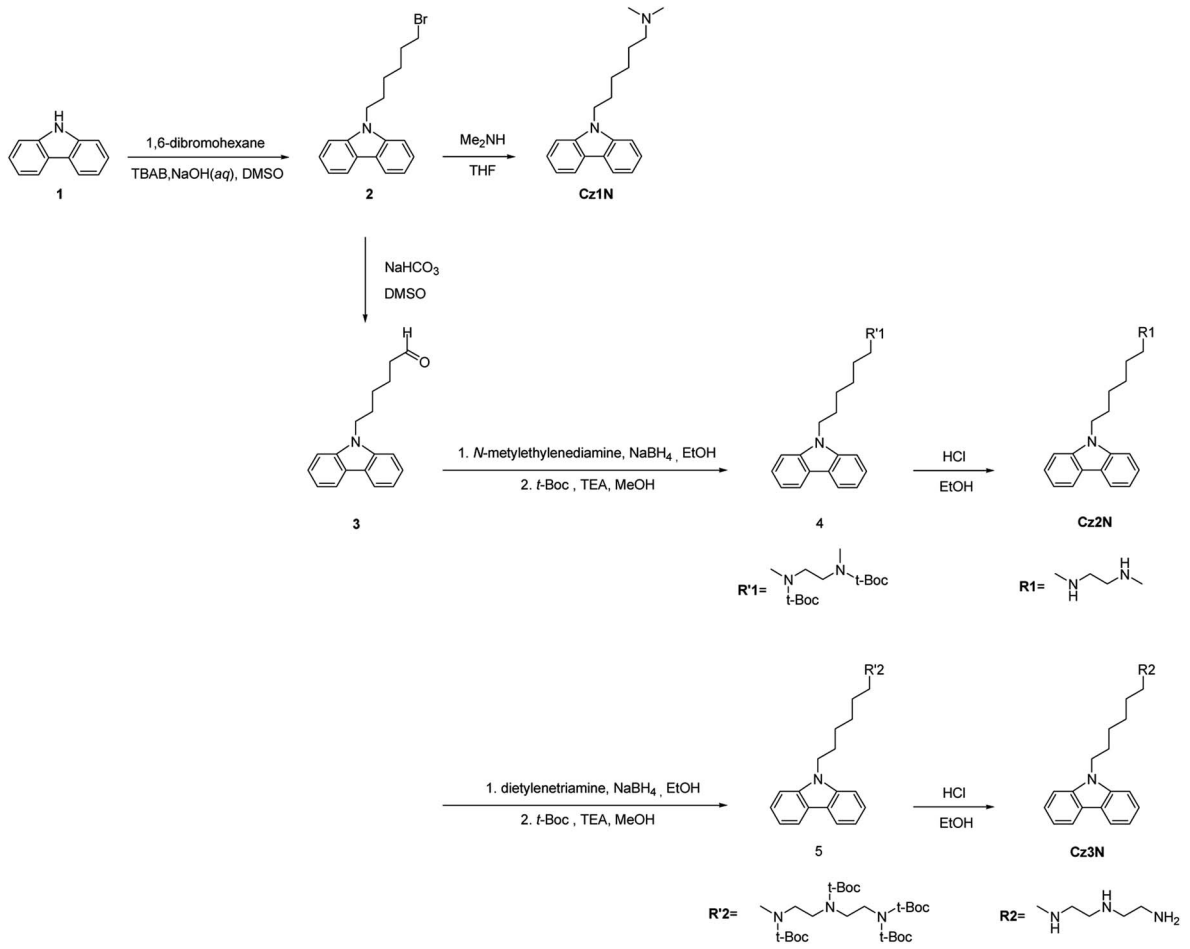

Scheme 1 Synthetic routes for the small molecules.

−3.05, −3.04 eV, respectively. The estimated band gaps of **Cz1N**, **Cz2N**, and **Cz3N** were 3.80, 3.98, and 4.00 eV, respectively. Although the band gaps of each material from the optical absorption spectra and CV measurements were marginally different, typically it is accepted that there is a difference between the optical band gap and electrochemical band gap of organic materials.[46,47] As observed in the absorption spectra of solid films, the difference of the HOMO for each material was also very small (see Fig. S5† and Table S2†).

Device characterization

Fig. 1(a) illustrates the single-step fabrication method of the BHJ/**CzxN** layer on an ITO substrate, and Fig. 1(b) exhibits the chemical structures of the electron donor, poly([2,6′-4,8-di(5-ethylhexylthienyl)benzo[1,2-b;3,3-b]dithiophene]{3-fluoro-2[(2-ethylhexyl)carbonyl]thieno[3,4-b]thiophenediyl}) (PTB7-Th), electron acceptor, phenyl-C_{71} butyric acid methyl ester ($PC_{71}BM$), and electron transporting materials, **Cz1N**, **Cz2N** and **Cz3N**, used in this study. Inverted BHJ organic solar cells were prepared with the configuration of ITO/PTB7-Th : PC_{71}-BM : **CzxN**/MoO_x/Ag, in which the **CzxN** layer with a different number of amine groups (1 to 3) was introduced, *via* spontaneous phase separation, to examine the effect on the device performance. To clarify the function of **CzxN**s in the BHJ solar cells, we also fabricated the reference device: ITO/PTB7-Th : $PC_{71}BM/MoO_x$/Ag. Fig. 2(a) exhibits the current density–voltage (*J*–*V*) characteristic curves of devices containing different **CzxN**s, and the corresponding device performances are summarized in Table 1. The device without **CzxN** yielded an average PCE of less than 1% with an extremely low V_{OC} of 0.13 V. This low V_{OC} value can be ascribed to the high-energy barrier between the LUMO value of $PC_{71}BM$ and the work function of ITO, which hinders the formation of ohmic contact at the interface. Interestingly, on adding a small amount of **CzxN**s, including **Cz1N**, **Cz2N**, and **Cz3N**, the PCE is increased from 0.24% to 4.91%. (For the best champion device, the PCE increased from 0.53% to 5.67%). This is attributed to the formation of an ETL, which induces a substantially decreased WF of ITO *via* the development of interfacial dipoles and reduces the energy barrier between the BHJ and ITO substrate as shown in Fig. 2(b). Additionally, we also performed impedance spectroscopy exhibiting a significantly decreased internal resistance on increasing the number of amine groups in the **CzxN**s: **Cz3N** (145 Ω) < **Cz2N** (158 kΩ) < **Cz1N** (200 kΩ) as shown in Fig. 2(d). Typically, a reduced internal resistance in BHJ solar

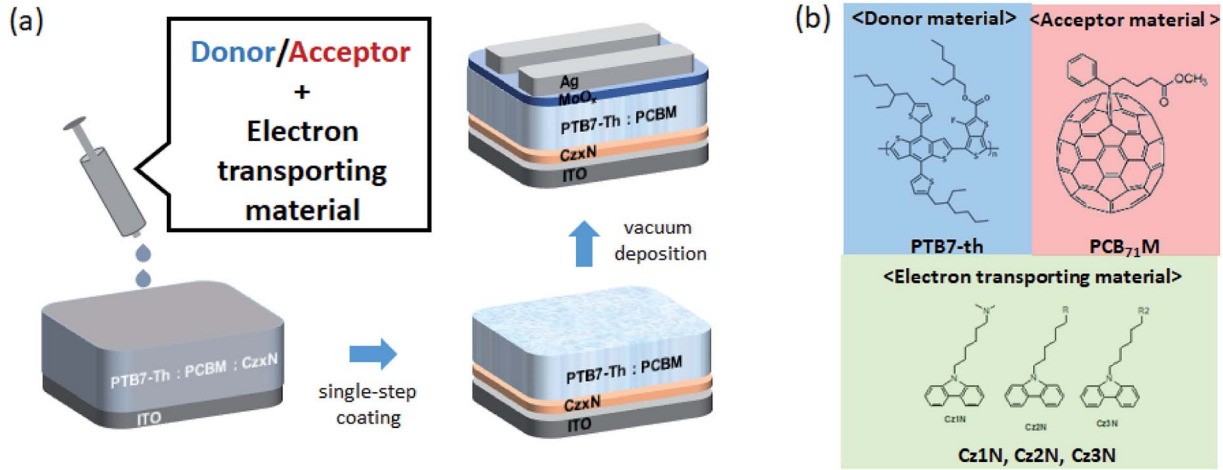

Fig. 1 (a) Schematic diagram of the single-step process for fabricating a BHJ layer, including vacuum deposition on an ITO substrate. (b) Chemical structure of the electron donor, acceptor and electron transporting layer used in this study.

cells can be ascribed to a decrease of the bulk resistance of BHJ films or a decrease of the series resistance at the interface between the ETL and active layers. The bulk resistance of BHJ films is also significantly related to the change of surface morphology of the BHJ films. Therefore, we observed the surface morphology of the **CzxN** : BHJ films by using the

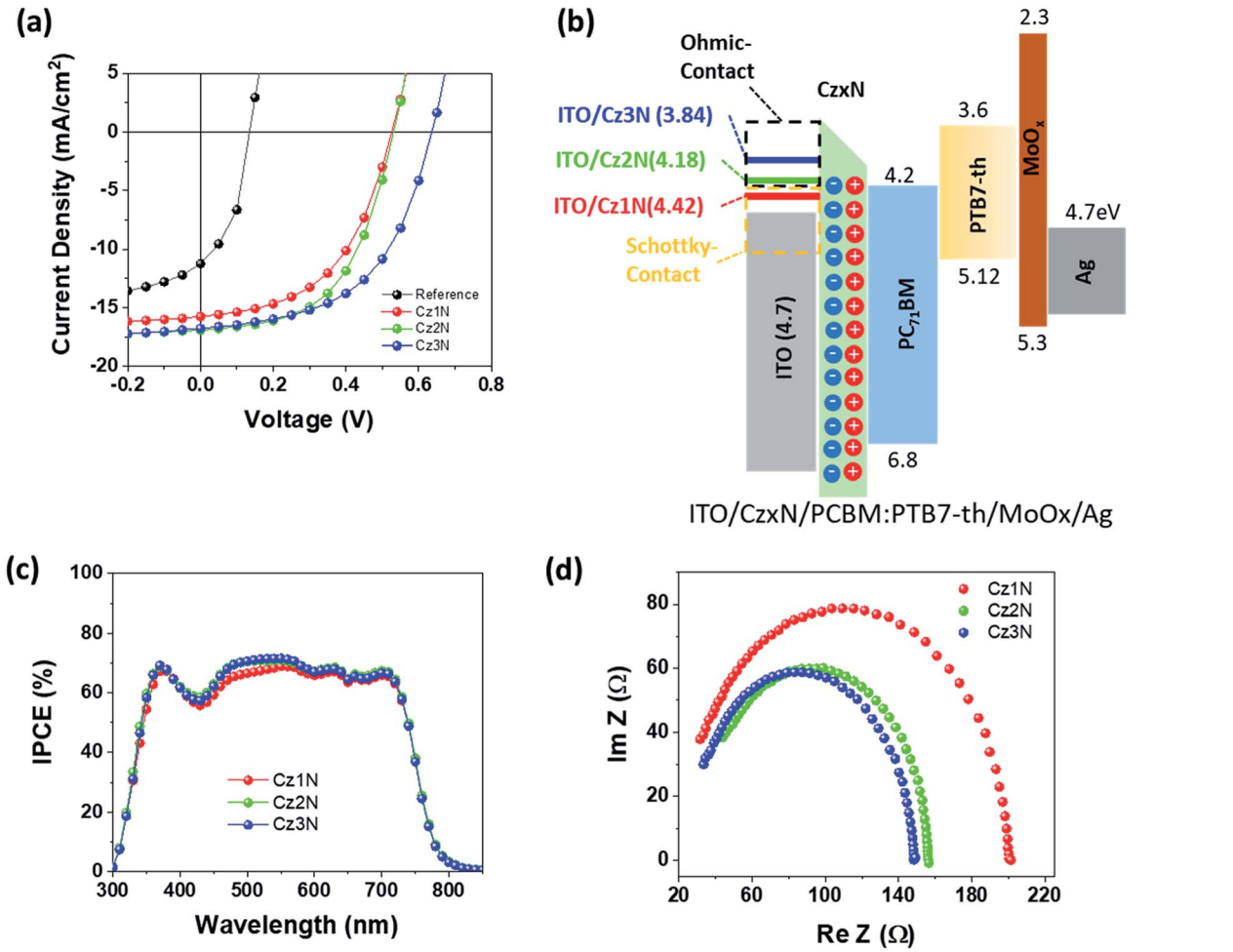

Fig. 2 (a) Current density–voltage (*J*–*V*) characteristic curves, (b) energy level diagram, (c) the Incident Photon-to-Electron Conversion Efficiency (IPCE) spectra and (d) Nyquist plots of the devices from the impedance spectroscopy of the devices with different conjugated small molecules containing a number of amine groups from 1 to 3 (Resistance (Re Z), Impedance (Im Z)).

Table 1 Photovoltaic properties of the **CzxNs** : BHJ blend based solar cells. The mean values of each parameter (V_{OC}, J_{SC}, FF, and PCE) with the standard deviation were calculated on the basis of 20 devices

Interlayer	V_{OC} (V)	J_{SC} (mA cm^{-2})	FF (%)	PCE (%)	J_{SC}[a] (mA cm^{-2})$_{IPCE}$
None	0.13 ± 0.04	6.70 ± 0.60	0.28 ± 0.02	0.24 ± 0.12	
Cz1N	0.50 ± 0.01	14.90 ± 0.52	0.48 ± 0.02	3.81 ± 0.37	14.00
Cz2N	0.55 ± 0.07	15.10 ± 0.86	0.51 ± 0.05	4.21 ± 0.41	16.05
Cz3N	0.60 ± 0.04	15.50 ± 0.89	0.53 ± 0.02	4.91 ± 0.35	15.46

[a] is integrated J_{SC} from the IPCE spectra.

tapping mode of atomic force microscopy (AFM). As shown in Fig. S6(a)–(c),† despite slightly different surface morphologies, it can be noticed that the small grains in the BHJ films were almost similar in the AFM images. This result is well consistent with the trend of J_{SC} values obtained in the *J*–*V* characteristics (small change of J_{SC} value from **Cz1N** to **Cz3N**, see Table 1); the surface morphology of the BHJ films is not significantly influenced by changing the number of amine groups on the CSEs. With this result and KP measurements for **CzxNs**, it can be concluded that the effect of the interface is more dominant for the decrease of the resistance in the device. Therefore, the charge recombination in the **CzxN** : BHJ devices is reduced. Even though the best PCE values of PTB7-Th/$PC_{71}BM$ with the standard ETL system are higher than our resulting data, our method has the merit of eliminating one of the processing steps. So, this type of material, for the formation of an ETL by using spontaneous phase separation, should be consistently researched, especially for roll-to-roll processes. The photovoltaic properties of the PTB7-Th-based BHJ solar cells with a standard ETL are included in the ESI.†

Mechanism

In order to gain an insight into the formation of the vertically self-assembled ETL of **CzxNs** *via* a single-step coating process, we investigated the location of the **CzxN** layer in the ITO/**CzxN** : BHJ structure using time-of-flight secondary-ion mass spectroscopy (ToF-SIMS), which allowed the distribution of the composition along the depth of the film to be detected. Fig. 3(a)–(c) exhibit the ToF-SIMS depth profiles of the ITO/**CzxN** : BHJ structure. Each material, including ITO, **CzxN** and PTB7-Th, has been tracked

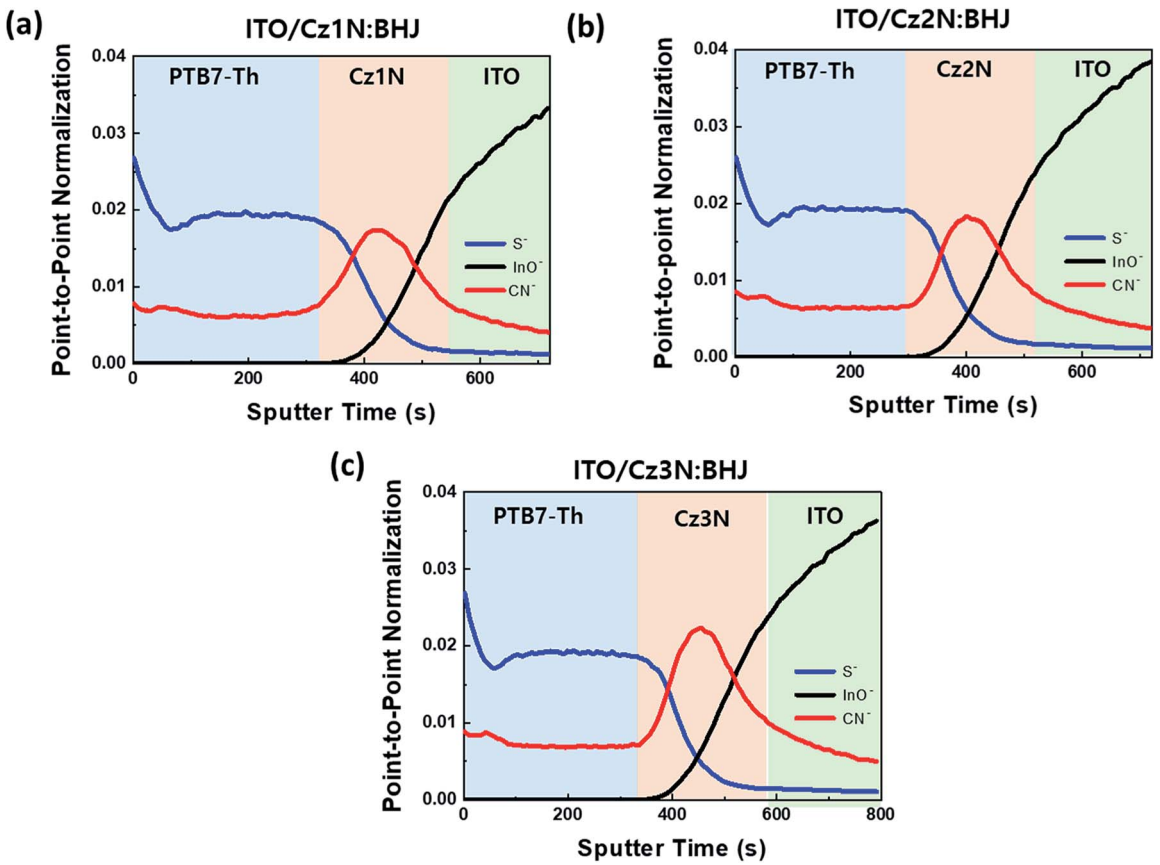

Fig. 3 ToF-SIMS depth profiles for (a) ITO/**Cz1N** : BHJ, (b) ITO/**Cz2N** : BHJ and (c) ITO/**Cz3N** : BHJ.

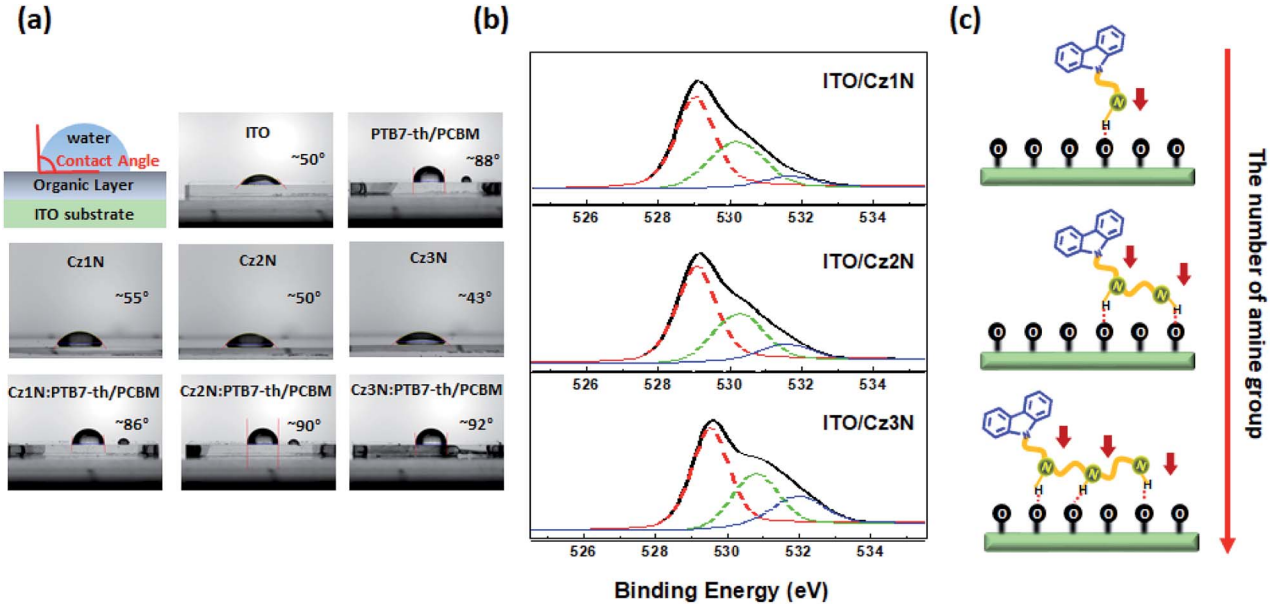

Fig. 4 (a) Water contact angle measurement, (b) high-resolution XPS deconvoluted spectra of O 1s for ITO/**CzxN**s and (c) the concept of spontaneous phase separation of conjugated small molecules.

down with their unique ions. The S^- and InO^- are assigned to the PTB7-Th and ITO, respectively, and the CN^- ion is attributed to the existence of **CzxN**s. The accumulation of CN^- ions, with high intensity, at the interface between the ITO and BHJ layer was monitored, which shows the formation of the **CzxN** layer by spontaneous vertical phase separation during the single-step coating process of the **CzxN** : BHJ blend solutions. This phenomenon of spontaneous vertical phase separation may be attributed to the high surface energies of the **CzxN**s relative to the BHJ components. Therefore, these results show that the introduction of **CzxN**s, which have a conjugated portion and amine groups in one molecules, in a one-step process has the advantage of reduction of the processing steps.

To support the formation of a **CzxN** self-assembled layer on top of the ITO substrate and the absence of **CzxN** in the self-assembled BHJ layer, water contact angle measurements of the samples (described in methods) have been carried out. Fig. 4(a) shows snapshots of a water droplet on the bare ITO substrate, BHJ film, **CzxN** films and **CzxN** : BHJ films on ITO, respectively. From this data, it can be concluded that the hydrophilic property of the films increased with the increase of the number of amine groups (**Cz1N** < **Cz2N** < **Cz3N**, 55° > 50° > 43°), whereas the **CzxN** : BHJ films show strong hydrophobic properties with the increase of the number of amine groups (**Cz3N** : BHJ > **Cz2N** : BHJ > **Cz1N** : BHJ, 92° > 90° > 86°). This is because of not only the presence of amine groups in the **CzxN**s, which lead to hydrophilicity, but also the non-polar chemical composition from the BHJ materials having hydrophobicity. We also note that the hydrophobicity of the **CzxN** : BHJ films is relatively similar to that of the BHJ film itself. That is, the uppermost surface contains no **CzxN**s, indicating that the vertical self-assembly process for the BHJ/**CzxN** bi-layered structure occurred during film formation (Table 2).

To understand the interaction between the **CzxN**s and ITO substrate during the single-coating process, we carried out X-ray photoelectron spectroscopy (XPS) measurements on the three

Table 2 Deconvolution results of XPS spectra of the ITO/**CzxN**s

Interlayer	Position (eV)	% Relative intensity	FWHM (eV)	GL[a] (%)	Area (P) CPS (eV)	Assignment
Cz1N	529.63	58.63	1.17	41	124139	In–O
	530.68	34.31	1.64	0	72 642	Sn–O
	532.03	7.07	1.51	0	14 962	O–H, O–C and $(O_2)^{2-}$
Cz2N	529.68	58.14	1.18	36	80 434	In–O
	530.76	31.24	1.52	2	43 222	Sn–O
	531.93	9.77	1.48	0	13 522	O–H, O–C and $(O_2)^{2-}$
Cz3N	529.49	54.17	1.24	34	51 857	In–O
	530.75	28.83	1.50	0	27 597	Sn–O
	531.94	17.00	1.67	0	16 279	O–H, O–C and $(O_2)^{2-}$

[a] GL: % Lorentzian–Gaussian.

different **CzxN** layers (**Cz1N**, **Cz2N** and **Cz3N**)/ITO substrates. As shown in Fig. 4(b), the O 1s core level XPS spectra are presented as solid lines, while the deconvolutions of the O 1s spectra with Gaussian peaks are presented as dashed lines. The O 1s core level signals were successfully fitted to three peaks corresponding to the In–O (BE = 529.5 eV), Sn–O (BE = 530.7 eV) and chemically adsorbed O–H bonding (BE = 531.9 eV), respectively.[48–51] As compared to **Cz1N** and **Cz2N**, **Cz3N** exhibited higher intensity of the peak at 531.9 eV corresponding to the chemically adsorbed O–H bonds, indicating that the increase of the number of amine groups effectively provides more chemically adsorbed O–H bonds, which implies that the interfacial interaction between the amine groups and the ITO was increased. The **CzxN**s have protons attached to the electro-negative nitrogen atoms, which work as the hydrogen bonding donors toward the electro-negative oxygen atoms, which work as the hydrogen bonding acceptors, at the surface of ITO.

Conclusions

We designed and synthesized carbazole-based CSEs, **Cz1N**, **Cz2N** and **Cz3N**, with different numbers of amine groups, by reductive amination reaction to achieve the spontaneous phase separation of the amine-containing CSEs for the automatic formation of an ETL layer, out of one solution containing the bulk-heterojunction materials and CSEs. A strong interfacial dipole caused by the hydrogen bonding between the amine groups of the small molecules and ITO is formed at the interface of ITO/**CzxN**s, leading to a decrease of the effective WF of ITO. **Cz3N** showed the lowest WF of ITO and series resistance at the interface caused by more hydrogen bonding interaction with ITO as confirmed by XPS.

Spontaneous phase separation generated the automatic formation of the bulk-heterojunction layer and electron transporting **CzxN** interlayer when one solution containing **CzxN** and BHJ materials was spin-casted on ITO, which was verified by performing ToF-SIMS elemental depth profiles. When the number of amine groups was increased, the device performance was enhanced caused by more effective spontaneous phase separation, and lower WF of ITO and impedance. It was demonstrated that increasing the number of amine groups in the CSEs (from **Cz1N** to **Cz3N**) enhanced the hydrogen bonding between the **CzxN**s and ITO, as confirmed by XPS, and provides higher PCE. These results show that the introduction of **CzxN**s in one-step processing by using spontaneous phase separation has the advantage of enabling the reduction of the processing steps. By optimizing the structure of the CSE *via* the introduction of a more efficient electron transporting conjugated moiety and modification of the side chain, it could be possible to realize a more practical procedure for device fabrication.

Experimental section

Materials

All reagents were purchased from Aldrich or TCI, and used without further purification. ^{1}H/^{13}C NMR spectra were recorded by a Varian Gemini-300 spectrometer (recorded in ppm units). High resolution mass spectra (HRMS) were recorded on a JEOL JMS-700 mass spectrometer under electron impact (EI) or fast atom bombardment (FAB) conditions at the Korea Basic Science Institute (Daegu).

Synthesis of monomers and small molecules

9-(6-Bromo-hexyl)-9*H*-carbazole (2). To a mixture of 9*H*-carbazole (**1**) (5 g, 29.9 mmol), tetrabutylammonium bromide (TBAB) (cat.) and a solution of NaOH (6.0 g, 149.5 mmol, in 10 ml of H_2O) in 100 ml of dimethyl sulfoxide (DMSO) was added 1,6-dibromohexane (3.7 ml, 23.9 mmol) at 40 °C. After completion of the addition, the reaction mixture was stirred for 10 min at 40 °C. After pouring into 100 ml of H_2O, the reaction mixture was extracted with 2 × 100 ml of $CHCl_3$. The combined organic phase was washed with 3 × 100 ml of water. The organic phase was concentrated under reduced pressure and purified by flash column chromatography to give 3.8 g (38%) of compound **2** as a white solid. ^{1}H NMR (300 MHz, $CDCl_3$): δ (ppm) 8.13 (d, 2H, J = 7.7 Hz) 7.49 (t, 2H, J = 7.7 Hz) 7.42 (d, 2H, J = 8.2 Hz) 7.25 (t, 2H, J = 7.6 Hz) 4.32 (t, 2H, J = 7.0 Hz) 3.37 (t, 2H, J = 7.0 Hz) 1.91 (qi, 2H, J = 7.6 Hz) 1.83 (qi, 2H, J = 7.6 Hz) 1.55–1.35 (m, 4H); ^{13}C NMR (75 MHz, $CDCl_3$): δ (ppm) 140.42, 125.70, 122.86, 120.46, 118.85, 108.68, 42.87, 33.92, 32.62, 28.88, 27.98, 26.51. HRMS (m/z, EI$^+$) calcd for $C_{18}H_{20}BrN$, 329.0779, found 329.0776.

6-Carbazol-9-yl-hexanal (3). To a solution of $NaHCO_3$ (5 g, 10.2 mmol) in 10 ml of dimethyl sulfoxide (DMSO) was added compound **2** (2 g, 6.0 mmol) at 120 °C. The reaction mixture was stirred for 30 min at 120 °C. After pouring into 100 ml of H_2O, the reaction mixture was extracted with 2 × 100 ml of ethyl acetate. The combined organic phase was washed with 3 × 100 ml of water. The combined organic phase was concentrated under reduced pressure and purified by flash column chromatography to give 0.6 g (33%) of compound **3** as a white solid. ^{1}H NMR (300 MHz, $CDCl_3$): δ (ppm) 9.72 (s, 1H) 8.11 (d, 2H, J = 7.7 Hz) 7.47 (t, 2H, J = 7.7 Hz) 7.39 (d, 2H, J = 8.3 Hz) 7.23 (t, 2H, J = 7.7 Hz) 4.31 (t, 2H, J = 7.1 Hz) 2.39 (t, 2H, J = 7.0 Hz) 1.91 (t, 2H, J = 7.7H) 1.65 (t, 2H, J = 7.6H) 1.50–1.35 (m, 2H); ^{13}C NMR (75 MHz, $CDCl_3$): δ (ppm) 202.36, 140.33, 125.65, 122.80, 120.40, 118.82, 108.59, 43.70, 42.75, 28.82, 26.80, 21.76. HRMS (m/z, FAB$^+$) calcd for $C_{18}H_{20}NO$, 266.1545, found 266.1541.

{2-[*tert*-Butoxycarbonyl-(6-carbazol-9-yl-hexyl)-amino]-ethyl}-methyl-carbamic acid *tert*-butyl ester (4). A solution of compound **3** (3.0 g, 9.1 mmol) and *N*-methylethylenediamine (0.78 ml, 9.1 mmol) in 20 ml of EtOH was stirred at 50 °C for 5 h. Then, the reaction mixture was treated with $NaBH_4$ (0.3 g, 9.1 mmol) and stirred overnight. After treating under reduced pressure to remove EtOH, the reaction mixture was extracted with 2 × 100 ml of ethyl acetate. The combined organic phase was washed with 3 × 50 ml of water. The organic phase was concentrated under reduced pressure. The crude product was treated with 3 ml of triethylamine and 25 ml of MeOH. After cooling to 0 °C, the reaction mixture was treated with di-*tert*-butyl dicarbonate (39.7 ml, 185.5 mmol) in 10 ml of MeOH and stirred for 1 h. After warming to room temperature, the mixture was stirred overnight. The reaction mixture was extracted with 2 × 50 ml of $CHCl_3$. The combined organic phase was washed

with 3 × 50 ml of water. The organic phase was purified by flash column chromatography to give 3.0 g (29%) of compound **4** as a white oil. ^{1}H NMR (300 MHz, $CDCl_3$): δ (ppm) 8.12 (d, 2H, J = 7.7 Hz) 7.47 (t, 2H, J = 7.6 Hz) 7.41 (d, 2H, J = 8.2 Hz) 7.23 (t, 2H, J = 7.1 Hz) 4.31 (t, 2H, J = 7.1 Hz) 3.64 (t, 2H, J = 7.7 Hz) 2.48 (t, 2H, J = 7.7 Hz) 2.33 (t, 2H, J = 7.7 Hz) 2.24 (s, 3H) 1.95–1.85 (m, 2H) 1.48 (s, 18H) 1.45–1.30 (m, 6H); ^{13}C NMR (75 MHz, $CDCl_3$): δ (ppm) 152.44, 140.39, 125.57 122.77 120.32, 118.70, 108.66, 82.13, 57.85, 55.54, 43.87, 42.98, 42.58, 28.99 28.07, 27.37, 27.29, 27.17. HRMS (m/z, EI$^+$) calcd for $C_{31}H_{45}N_3O_4$, 523.3410, found 523.3412.

[2-(2,2′-Di-*tert*-butoxycarbonyl-ethylamino)-ethyl]-(6-carbazol-9-yl-hexyl)-carbamic acid *tert*-butyl ester (5). The reaction mixture was reacted under the same conditions as compound **4** and the crude product was purified by flash column chromatography to give 2.2 g (16%) of compound **5** as a white oil. ^{1}H NMR (300 MHz, $CDCl_3$): δ (ppm) 8.09 (d, 2H, J = 7.6 Hz) 7.45 (t, 2H, J = 7.6 Hz) 7.38 (d, 2H, J = 7.6 Hz) 7.22 (t, 2H, J = 7.6 Hz) 4.29 (t, 2H, J = 7.0 Hz) 3.45–3.05 (m, 10H) 2.05–1.85 (m, 2H) 1.42 (s, 36H) 1.35–1.20 (m, 6H); ^{13}C NMR (75 MHz, $CDCl_3$): δ (ppm) 156.08, 155.26, 140.37, 125.57, 122.80, 120.32, 118.71, 108.59, 80.09, 79.48, 79.07, 47.68, 47.30, 46.72, 45.82, 45.26, 44.83, 42.94, 39.65, 39.47, 28.98, 28.38, 28.12, 27.10, 26.62. HRMS (m/z, FAB$^+$) $C_{42}H_{65}N_4O_8$, 753.4802, found 753.4799.

(6-Carbazol-9-yl-hexyl)-dimethyl-amine (Cz1N). A solution of compound **2** (2.0 g, 6.0 mmol) in 20 ml of tetrahydrofuran (THF) was treated with dimethylamine (30.2 ml, 60.6 mmol) at −78 °C and the mixture was stirred for 2 days under Ar. After pouring into 30 ml of NaOH (0.1 M), the reaction mixture was extracted with 2 × 50 ml of ethyl acetate. The combined organic phase was washed with 3 × 50 ml of water. The organic phase was concentrated under reduced pressure and purified by flash column chromatography to give 0.4 g (25%) of **Cz1N** as a bright yellow oil. ^{1}H NMR (300 MHz, $CDCl_3$): δ (ppm) 8.14 (d, 2H, J = 7.7 Hz) 7.49 (t, 2H, J = 7.7 Hz) 7.42 (d, 2H, J = 7.7 Hz) 7.26 (t, 2H, J = 7.7 Hz) 4.30 (t, 2H, J = 7.1 Hz) 2.30–2.20 (m, 2H), 2.21 (s, 6H) 1.92–1.85 (qi, 2H, J = 7.7 Hz) 1.52–1.30 (m, 6H); ^{13}C NMR (125 MHz, $CDCl_3$) δ (ppm) 140.41, 125.56, 122.80, 120.32, 118.70, 108.63, 59.69, 45.43, 42.99, 28.92, 27.54, 27.25, 27.24. HRMS (m/z, FAB$^+$) calcd for $C_{20}H_{27}N_2$, 295.2174, found 295.2177.

***N*-(6-Carbazol-9-yl-hexyl)-*N*′-methyl-ethane-1,2-diamine (Cz2N).** To a solution of compound **4** (1.8 g, 3.4 mmol) in 30 ml of EtOH was added 4 N HCl (55 ml, 220.0 mmol) dropwise at 0 °C. After stirring at room temperature overnight, the reaction mixture was treated with saturated NaOH (aq) to adjust the pH to around 11. After extraction of the reaction mixture with 2 × 100 ml of ethyl acetate, the combined organic phase was washed with 3 × 100 ml of water. The organic phase was concentrated under reduced pressure to give 0.4 g (24%) of **Cz2N** as a yellow oil. ^{1}H NMR (300 MHz, $CDCl_3$): δ (ppm) 8.11 (d, 2H, J = 7.6 Hz) 7.47 (t, 2H, J = 7.7 Hz) 7.41 (d, 2H, J = 7.7 Hz) 7.23 (t, 2H, J = 7.7 Hz) 4.31 (t, 2H, J = 7.0 Hz) 2.72 (t, 2H, J = 5.9 Hz) 2.35 (t, 2H, J = 5.8 Hz) 2.28 (t, 2H, J = 7.0 Hz) 2.20–2.05 (m, 2H) 2.16 (s, 3H) 1.95–1.80 (m, 2H) 1.55–1.30 (m, 6H); ^{13}C NMR (75 MHz, $CDCl_3$): δ (ppm) 140.41, 125.55, 122.80, 120.31, 118.70, 108.62, 60.52, 57.86, 43.00, 42.18, 39.56, 28.96, 27.25, 27.22, 27.15. HRMS (m/z, FAB$^+$) calcd for $C_{21}H_{30}N_3$, 324.2440, found 324.2437.

[2-(2-Amino-ethylamino)-ethyl]-(6-carbazol-9-yl-hexyl)-amine (Cz3N). The same conditions as for **Cz2N** were used to give 0.2 g (42%) of **Cz3N** as a yellow oil. ^{1}H NMR (300 MHz, $CDCl_3$): δ (ppm) 8.09 (d, 2H, J = 7.7 Hz) 7.45 (t, 2H, J = 7.0 Hz) 7.38 (d, 2H, J = 7.6 Hz) 7.21 (t, 2H, J = 7.7 Hz) 4.29 (t, 2H, J = 7.1 Hz) 2.77 (t, 2H, J = 5.7 Hz) 2.75–2.60 (m, 4H) 2.54 (t, 2H, J = 6.4 Hz) 1.85–1.60 (m, 2H) 1.55–1.45 (m, 8H); ^{13}C NMR (150 MHz, $CDCl_3$): δ (ppm) 140.36, 125.56, 122.74, 120.33, 118.68, 108.63, 52.46, 49.84, 49.49, 49.26, 42.98, 41.75, 29.97, 28.95, 27.25, 27.15. HRMS (m/z, FAB$^+$) calcd for $C_{22}H_{33}N_4$, 353.2705, found 353.2702.

Device fabrication and characterization

Solution preparation. The **CzxN** solutions were diluted in methanol to 0.2, 0.1 and 0.05 wt%. The blend solution of PTB7-Th : $PC_{71}BM$ was prepared by dissolving 7 mg of PTB7-Th and 10.5 mg of $PC_{71}BM$ (1 : 1.5 by weight) in 1 ml of chlorobenzene (CB) with a 1,8-diiodooctane (DIO) additive (3% by volume) and stirred overnight at 60 °C. The **CzxN** : BHJ solutions were prepared by mixing **CzxN** and the blend solutions (1 : 9 by volume).

Device fabrication. Inverted OPV (i-OPV) devices were fabricated with the structures of indium tin oxide (ITO) glass/**CzxN** : BHJ/MoO_x/Ag or ITO/BHJ/MoO_x/Ag. The coated ITO substrates were ultra-sonicated with deionized water, acetone and IPA for 20 minutes each, and then dried overnight in an oven at 85 °C. The ultra-sonicated ITO glass substrates were UV-Ozone treated for 20 minutes prior to device fabrication. For the i-OPV structures, the **CzxN** : BHJ or BHJ were spin-cast onto the ITO at 800 rpm for 30 seconds, followed by 5000 rpm for 10 seconds. Finally, MoO_x (2 nm) and Ag (120 nm) layers were deposited on the blend films *via* thermal evaporation under a high vacuum of 1 × 10^{-6} torr with a shadow mask. The active area of the devices was defined by the patterned Ag electrode (0.0464 cm^2).

Characterization. The performance of the solar cells, current *J*–*V* characteristics, was calibrated (with a 100 ms delay) using a Keithley 238 source measure unit (Keithley Instruments, Inc) under AM 1.5G (air mass 1.5G global) illumination with 100 mW cm^{-2} intensity (Newport, Class AAA solar simulator) without a UV filter. Moreover, the external quantum efficiency (EQE) spectra were measured using a solar cell spectral response QE/IPCE measurement system (PV measurements, Inc.). The IPCE measurements were performed without bias light. The impedance spectroscopy measurements of the OPVs were obtained using a galvanostat mode (PGSTAT30) under the same illumination conditions as for the calibration of the OPVs. The atomic force microscopy (AFM) images were obtained with a scanning probe microscope system (n-Tracer SPM, NanoFocus Inc.). ToF-SIMS experiments were performed with a ToF-SIMS 5 (ION-ToF GmbH, Münster, Germany) in the KBSI Busan Center by using a pulsed 30 keV Bi_3^+ primary beam with a current 0.55 pA. The analyzed area used in this work is a square of 200 μm × 200 μm. Negative ion spectra were internally calibrated using H^-, C^-, C_2^-, C_3^- and C_4^- peaks normalized to the respective secondary total ion yields. The depth profile is a square of 500 μm × 500

μm using Ar_n^+, with $n = \sim 1000$ atoms as sputter argon gas cluster ion particles at 2.5 keV. Furthermore, the work function (WF) was obtained with a Kelvin probe system (KP 6500 Digital Kelvin Probe). The surface chemical composition of the **CzxN**/ITO layer was investigated by an X-ray photoelectron spectrometer (XPS) model Theta Probe AR-XPS System (Thermo Fisher Scientific, U.K) in the KBSI Busan Center. The X-ray source was Al Kα (1486.6 eV), operating at 100 W. The XPS spectra were curve fitted with a mixed Gaussian–Lorentzian shape and Shirley background using the analysis software XPSPEAK 4.1.

Conflicts of interest

There are no conflicts to declare.

Acknowledgements

This research was supported by the Technology Development Program to Solve Climate Changes of the National Research Foundation (NRF) funded by the Ministry of Science, ICT & Future Planning (NRF-2015M1A2A2057510). H. K. acknowledges the financial support from the National Foundation of Korea (NRF) grant funded by the Korea Government (the Ministry of Science and ICT, MSIT) (NRF-2017R1A2B4012490). Also, this work was supported by a GIST Research Institute (GRI) grant funded by GIST in 2018.

References

1 R. Søndergaard, M. Hösel, D. Angmo, T. T. Larsen-Olsen and F. C. Krebs, *Mater. Today*, 2012, **15**, 36–49.
2 W. Liu, S. Liu, N. K. Zawacka, T. R. Andersen, P. Cheng, L. Fu, M. Chen, W. Fu, E. Bundgaard, M. Jørgensen, X. Zhan, F. C. Krebs and H. Chen, *J. Mater. Chem. A*, 2014, **2**, 19809–19814.
3 S. Khan, L. Lorenzelli and R. S. Dahiya, *IEEE Sens. J.*, 2015, **15**, 3164–3185.
4 Y.-W. Su, S.-C. Lan and K.-H. Wei, *Mater. Today*, 2012, **15**, 554–562.
5 P. M. Beaujuge and J. M. J. Frechet, *J. Am. Chem. Soc.*, 2011, **133**, 20009–20029.
6 H. Yao, L. Ye, H. Zhang, S. Li, S. Zhang and J. Hou, *Chem. Rev.*, 2016, **116**, 7397–7457.
7 Y. Li, *Acc. Chem. Res.*, 2012, **45**, 723–733.
8 M. Tanveer, A. Habi and M. B. Khan, *NUST J. eng. sci.*, 2013, **6**, 15–20.
9 H.-C. Liao, C.-C. Ho, C.-Y. Chang, M.-H. Jao, S. B. Darling and W.-F. Su, *Mater. Today*, 2013, **16**, 326–336.
10 F. Zhao, C. Wang and X. Zhan, *Adv. Energy Mater.*, 2018, 1703147.
11 Y. Liu, J. Zhao, Z. Li, C. Mu, W. Ma, H. Hu, K. Jiang, H. Lin, H. Ade and H. Yan, *Nat. Commun.*, 2014, **5**, 5293.
12 J. Xiong, B. Yang, C. Cao, R. Wu, Y. Huang, J. Sun, J. Zhang, C. Liu, S. Tao, Y. Gao and J. Yang, *Org. Electron.*, 2016, **30**, 30–35.
13 S. Nam, J. Seo, S. Woo, W. H. Kim, H. Kim, D. D. C. Bradley and Y. Kim, *Nat. Commun.*, 2015, **6**, 8929.
14 Y.-J. Noh, S.-I. Na and S.-S. Kim, *Sol. Energy Mater. Sol. Cells*, 2013, **117**, 139–144.
15 H.-C. Chen, S.-W. Lin, J.-M. Jiang, Y.-W. Su and K.-H. Wei, *ACS Appl. Mater. Interfaces*, 2015, **7**, 6273–6281.
16 H.-K. Lin, Y.-W. Su, H.-C. Chen, Y.-J. Huang and K.-H. Wei, *ACS Appl. Mater. Interfaces*, 2016, **8**, 24603–24611.
17 C. V. Hoven, A. Garcia, G. C. Bazan and T.-Q. Nguyen, *Adv. Mater.*, 2008, **20**, 3793–3810.
18 Y. Sun, J. H. Seo, C. J. Takacs, J. Seifter and A. J. Heeger, *Adv. Mater.*, 2011, **23**, 1679–1683.
19 A. Guerrero, S. Chambon, L. Hirsch and G. Garcia-Belmonte, *Adv. Funct. Mater.*, 2014, **24**, 6234–6240.
20 J. Kong, J. Lee, Y. Jeong, M. Kim, S.-O. Kang and K. Lee, *Appl. Phys. Lett.*, 2012, **100**, 213305.
21 X. Bulliard, S. Ihn, S. Yun, Y. Kim, D. Choi, J. Choi, M. Kim, M. Sim, J. Park, W. Choi and K. Cho, *Adv. Funct. Mater.*, 2010, **20**, 4381–4387.
22 W. Beek, M. Wienk, M. Kemerink, X. Yang and R. Janssen, *J. Phys. Chem. B*, 2005, **109**, 9505–9516.
23 S. Dkhil, D. Duché, M. Gaceur, A. Thakur, F. Aboura, L. Escoubas, J. Simon, A. Guerrero, J. Bisquert, G. Belmonte, Q. Bao, M. Fahlman, C. Ackermann, O. Margeat and J. Ackermann, *Adv. Energy Mater.*, 2014, **4**, 1400805–1400816.
24 Z. He, C. Zhong, S. Su, M. Xu, H. Wu and Y. Cao, *Nat. Photonics*, 2012, **6**, 591–595.
25 Y. Zhou, C. Fuentes-Hernandez, J. Shim, J. Meyer, A. J. Giordano, H. Li, P. Winget, T. Papadopoulos, H. Cheun, J. Kim, M. Fenoll, A. Dindar, W. Haske, E. Najafabadi, T. M. Khan, H. Sojoudi, S. Barlow, S. Graham, J.-L. Brédas, S. R. Marder, A. Kahn and B. A. Kippelen, *Science*, 2012, **336**, 327–332.
26 M. Song, J.-W. Kang, D.-H. Kim, J.-D. Kwon, S.-G. Park, S. Nam, S. Jo, S. Y. Ryu and C. S. Kim, *Appl. Phys. Lett.*, 2013, **102**, 143303.
27 D. Ma, M. Lv, M. Lei, J. Zhu, H. Wang and X. Chen, *ACS Nano*, 2014, **8**, 1601–1608.
28 J. Wang, K. Lin, K. Zhang, X.-F. Jiang, K. Mahmood, L. Ying, F. Huang and Y. Cao, *Adv. Energy Mater.*, 2016, **6**, 1502563.
29 J. Lee, H. Kang, S. Kee, S. H. Lee, S. Y. Jeong, G. Kim, J. Kim, S. Hong, H. Back and K. Lee, *ACS Appl. Mater. Interfaces*, 2016, **8**, 6144–6151.
30 Z. Li, Y. Liu, K. Zhang, Z. Wang, P. Huang, D. Li, Y. Zhou and B. Song, *Langmuir*, 2017, **33**, 8679–8685.
31 H. Zhao, Y. Luo, L. Liu, Z. Xie and Y. Ma, *Mater. Chem. Front.*, 2017, **1**, 1087–1092.
32 Y.-M. Chang, R. Zhu, E. Richard, C.-C. Chen, G. Li and Y. Yang, *Adv. Funct. Mater.*, 2012, **22**, 3284–3289.
33 S. Dong, Z. Hu, K. Zhang, Q. Yin, X. Jiang, F. Huang and Y. Cao, *Adv. Mater.*, 2017, **29**, 1701507.
34 T. Schmaltz, G. Sforazzini, T. Reichert and H. Frauenrath, *Adv. Mater.*, 2017, **29**, 1605286.
35 J. Vinokur, B. Shamieh, I. Deckman, A. Singhal and G. L. Frey, *Chem. Mater.*, 2016, **28**, 8851–8870.

36 J. Lee, J. Kim, C.-L. Lee, G. Kim, T. K. Kim, H. Back, S. Jung, K. Yu, S. Hong, S. Lee, S. Kim, S. Jeong, H. Kang and K. Lee, *Adv. Energy Mater.*, 2017, **7**, 1700226.
37 H. Kang, J. Lee, S. Jung, K. Yu, S. Kwon, S. Hong, S. Kee, S. Lee, D. Kim and K. Lee, *Nanoscale*, 2013, **5**, 11587–11591.
38 H. Kang, S. Kee, K. Yu, J. Lee, G. Kim, J. Kim, J.-R. Kim, J. Kong and K. Lee, *Adv. Mater.*, 2015, **27**, 1408–1413.
39 H. Kang, S. Hong, J. Lee and K. Lee, *Adv. Mater.*, 2012, **24**, 3005–3009.
40 S. Kim, H. Kang, S. Hong, J. Lee, S. Lee, B. Park, J. Kim and K. Lee, *Adv. Funct. Mater.*, 2016, **26**, 3563–3569.
41 Z. Gao, Y. Zheng, Z. Wang and J. Yu, *J. Lumin.*, 2018, **201**, 359–363.
42 F.-C. Wu, K.-C. Tung, W.-Y. Chou, F.-C. Tang and H.-L. Cheng, *Org. Electron.*, 2016, **29**, 120–126.
43 L. Qiu, L. K. Ono, Y. Jiang, M. R. Leyden, S. R. Raga, S. Wang and Y. Qi, *J. Phys. Chem. B*, 2018, **122**, 511–520.
44 W. Lee, S. Jeong, C. Lee, G. Han, C. Cho, J.-Y. Lee and B. J. Kim, *Adv. Energy Mater.*, 2017, **7**, 1602812.
45 Z. Wu, C. Sun, S. Dong, X. F. Jiang, S. Wu, H. Wu, H. L. Yip, F. Huang and Y. Cao, *J. Am. Chem. Soc.*, 2016, **138**, 2004–2013.
46 A. Misra, P. Kumar, R. Srivastava, S. K. Dhawan, M. N. Kamalasanan and S. Chandra, *Indian J. Pure Appl. Phys.*, 2005, **43**, 921–925.
47 R. Heuvel, J. J. Franeker and R. A. J. Janssen, *Macromol. Chem. Phys.*, 2017, **218**, 1600502.
48 J. F. Moulder, W. F. Strickle, P. E. Sobol and K. D. Bomben, *Handbook of X-Ray Photoelectron Spectroscopy*, Perkin-Elmer, Eden Prairie, MN, 1992.
49 K. H. Lee, H. W. Jang, K.-B. Kim, Y.-H. Tak and J.-L. Lee, *J. Appl. Phys.*, 2004, **95**, 586–590.
50 H. Estrade-Szwarckopf, B. Rousseau, C. Herold and P. Lagrange, *Mol. Cryst. Liq. Cryst.*, 1998, **310**, 231–236.
51 K.-W. Tsai, S.-N. Hsieh, T.-F. Guo, Y.-J. Hsu, A. K.-Y. Jene and T.-C. J. Wen, *J. Mater. Chem. C*, 2013, **1**, 531–535.